Aviation Sustainability Through Hyperspectral Image Analysis Methodology for Aircraft-Induced Clouds

Amy Rose, Lance Sherry

Center for Air Transportation Systems Research at George Mason University, Fairfax, VA

Abstract: Ninety-eight percent (98%) of anthropogenic global heating is the result of Green House gases (GHG). The remaining 2% is attributed to the Global Heating effects of Aircraft Induced Clouds (AIC). AIC form from soot and water vapor emitted from jet engines at high altitudes in favorable atmospheric conditions. The AIC absorb, scatter, and reflect back to Earth, the outgoing longwave radiation results in increased temperatures. This radiation would otherwise escape to space resulting in no warming effect.

Reducing AIC would have an immediate impact on the Earth's temperature structure, unlike GHGs which take between 20 and 40 years to have an impact. Researchers have proposed an AIC Abatement Program (AAP) to modify flight plans without additional fuel burn or CO2 emission costs to reduce AICs. A critical component of the technology to enable AAP is the ability to accurately identify AIC from publicly available aerial and satellite images.

This paper describes a method for hyperspectral analysis of aerial images to accurately identify AIC, based on naturally-formed altostratus and cumulus clouds. The method, a case study, and future work are provided.

1 INTRODUCTION

Ninety-eight percent (98%) of anthropogenic global heating is the result of Green House gases (GHG) [1]. The remaining 2% is attributed to the Global Heating effects of Aircraft Inducted Clouds (AIC).

AIC are generated when soot and water vapor are emitted from jet engines into atmospheric conditions that meet the Schmidt-Appleman Criteria (i.e. -42 degrees F and 100% humidity). The water vapor bonds to the soot particles and creates ice crystals. The ice crystals grow and replicate forming cirrus-like clouds.

AIC absorb, scatter, and reflect back to the Earth an estimated 33% of the outgoing longwave radiation emitted by the Earth that is directed at the AIC. This radiation, that would otherwise be transmitted out to space, results in an increase in the Earth's temperature structure [2]. AIC also can provide a cooling effect, reflecting 23% of the incoming shortwave radiation back out to space. The cooling effect only takes place in daylight hours and is a function of the Sun's angle of azimuth. Note: on aggregate, during daylight, AIC has a net warming effect (33% - 23% = 10%).

Whereas the effect on the lower atmosphere temperature structure of CO2 and other Green House Gases is apparent 20 to 40 years from the date it is emitted, the effect of AIC is immediate. For these reasons, it may behoove the industry to develop plans to mitigate the global warming effects of AIC.

In the U.S. airspace, AIC are generated by an average of only 15% of the daily flights (max 34%) [3]. The location of the AIC is dependent on atmospheric conditions, known as Ice Super Saturated Regions (ISSRs), and occur mostly in the south-eastern and mid-Atlantic region of the United States and on the Pacific Coast.

AIC formation can be avoided by increasing the cruise flight level by between 2,000 and 4,000 feet. Due to low air density at cruise flight levels, the additional fuel burn required to climb to the higher cruising altitude is mitigated by reduced fuel burn due to reduced drag at the higher cruising altitude. Similar results were reported by Teoh et.al. [4] for Japanese airspace, and Rosenow et. al. [5] and Kaiser et.al. [6] for European airspace.

These results indicate the feasibility of an AIC Abatement Program (AAP) to mitigate the effects of aviation's anthropogenic effects on global warming [7]. To facilitate the proposed AAP, it is necessary to inventory AIC in the National Airspace. Recent public availability of satellite images makes it possible to generate real-time and historic AIC Inventories, albeit limitedly. Such limitations are outlined in Section 2.

This paper describes a method for hyperspectral analysis of aerial images to identify AIC based on the analysis of altostratus and cumulus clouds. The method includes 5 steps: the elimination of noisy bands, identification and overlay of primary regions of interest, creation of a spectral library based on in-scene spectra, running of algorithm with in-scene spectra on image, and the isolation of clouds with histogram stretching and color table manipulation.

Cloud types are defined primarily by the altitude range in which they form (low, middle, high) because of the climatic and meteorological conditions associated with the regions of the atmosphere. Such conditions include temperature, barometric pressure, lapse rate, stability, and relative humidity. From these factors, it is possible to predict cloud type, which is notably useful in the prediction of AIC formation.

The process is demonstrated with an aerial image from AVIRIS Classic flight f100906t01, Donaldson Plantation Flight Line 1. The location is Gainesville, Florida, September 6, 2010 at 18:29 UTC (14:29 EDT) and pixel size is 3.6 meters. Images were processed using the Matched Filter (MF), Adaptive Coherence Estimator (ACE), and Principal Components Analysis (PCA) algorithms. Image preprocessing and analysis were completed with L3 Harris ENVI Classic version 5.5.3.

This paper is organized as follows: Section 2 describes the overall process for generating AIC Inventories from hyperspectral images and the special role of spectral analysis. Section 3 describes the methods for spectral analysis. Section 4 provides results of spectral analysis of the NASA Airborne Visible/Infrared Imaging Spectrometer (AVIRIS) hyperspectral image. [8] Section 5 discusses the implications of these results and future work.

2 IMAGES AND SPECTRAL ANALYSIS FOR AIC INVENTORY

Researchers have proposed an AIC Abatement Program (AAP) to mitigate the effects of aviation's anthropogenic effects on global warming [7]. A critical component of the infrastructure to support the AIC AAP is to inventory AIC in the National Airspace Systems (NAS) at some periodic basis (e.g. once per hour). The need for high spatial resolution led to the selection of hyperspectral (AVIRIS) data for this study. Other researchers ([9]-[16]) have used neural networks and deep learning for AIC identification and the consensus is that this is not sufficient due to spatial and spectral resolution constraints. These researchers have identified domain skills in remote sensing, atmospheric physics, and aviation as gaps.

AIC inventory in the NAS can be conducted by one of two ways. First flight tracks can be overlayed on Ice Super Saturated Regions (ISSRs) identified by processing of atmospheric data [17]. Based on AIC formation and persistence criteria, such as Schmidt-Appleman, AIC can be assumed to be formed and persist. Second, by analysis of satellite and other high altitude imagery AIC can be identified. The AIC identification in the images can be done directly by hyperspectral image analysis (as described in this paper,) or by machine learning algorithms. To train/test the machine learning (ML) algorithms, the images with and without AIC must be semantically annotated. Manual approaches are time consuming and exhibit poor reliability (inter and intra). Hyperspectral image analysis (as described in this paper) could be used to perform automated image annotation of AIC for ML training and testing.

This study provides analysis of hyperspectral aerial imagery. The main disadvantage is that it exhibits less spatiotemporal coverage than multispectral satellite imagery. The main

advantage is significantly higher spatial and spectral resolution. Works on current research and plans for future research all aimed at improving reliability of AIC detection is outlined in Figure 1. Researchers have proposed using 3 methods to verify the presence of an AIC in the image: (1) hyperspectral remote sensing, (2) coexistence with an ISSR, and (3) coexistence with flight tracks. The 3 methods are color-coded in the Dissertation Scope image in light blue, medium blue, and dark blue, respectively.

The process for combined atmospheric data analysis and satellite/high altitude image analysis is summarized in Figure 1. The upper row from left to right shows the conversion of Hyperspectral Images to Exploitation Ready Images to identification of Cirrus clouds. This is accomplished using In-Scene Spectra and Spectral Imagery Analysis. Natural cirrus clouds can be distinguished from AIC by overlaying flight track data.

The lower row uses atmospheric data and flight track data, along with AIC formation and persistence models to estimate the presence of AIC.

The results of the analysis of the image analysis and the atmospheric analysis can be combined. The resulting identification of an AIC can be assigned a confidence level to capture the accuracy of the analytical methods.

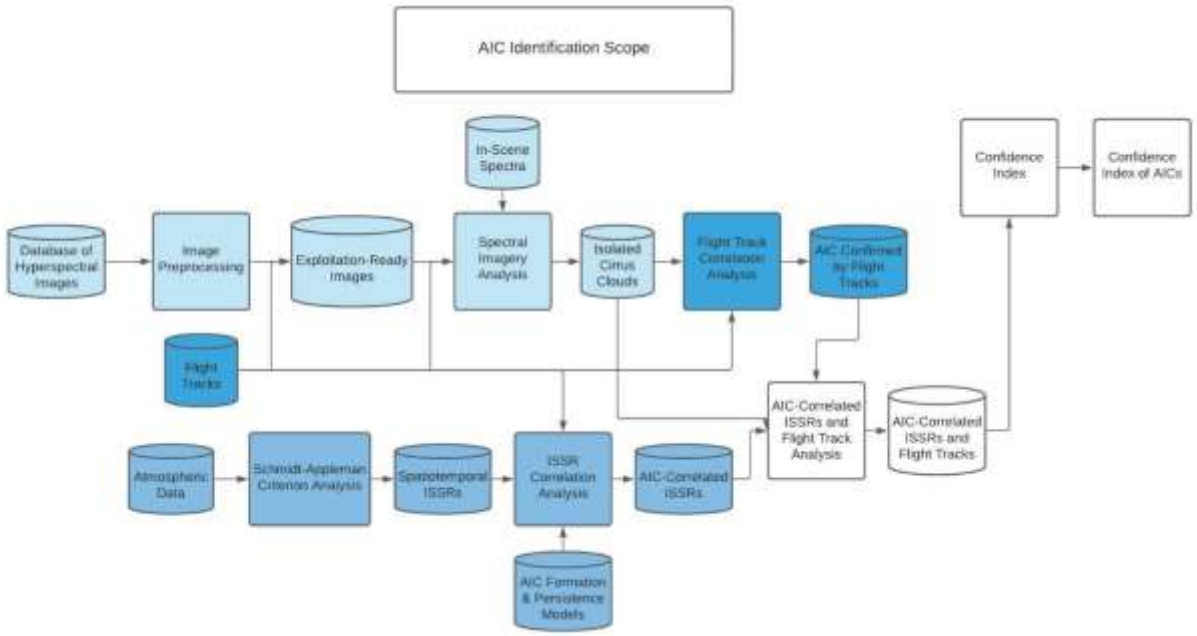

Figure 1. AIC Identification Scope Block Diagram

Hyperspectral Image Processing

The hyperspectral concept refers to a relatively high precision means of obtaining spectral information without physical contact. Spectral scientists have classified several bands of the electromagnetic spectrum with similar characteristics. Hyperspectral measurements have hundreds of narrow bands while multispectral measurements have several wide bands. The advantages of using a hyperspectral sensor are higher levels of contiguity, modernity, specificity, resolution, and precision. The disadvantages are higher cost, less spatial

and temporal coverage, longer preprocessing times, and less common, which could all serve as barriers to entry for students, academics, and other stakeholders. An example of a hyperspectral sensor is NASA AVIRIS Classic with 224 continuous bands between 0.38 and 2.510 micrometers.

3 METHOD FOR HYPERSPECTRAL ANALYSIS OF AIC

The method for Hyperspectral Analysis of AIC takes a raw image (before pro-processing) and converts the image to isolate the AIC (Figure 2). This is a 5 step process:

1. Eliminate Noisy Bands
2. Identify and Overlay Primary Regions of Interest
3. Create Spectral Library based on In-Scene Spectra
4. Run Algorithms (MF, ACE, PCA) with In-Scene Spectra on Image
5. Isolate Clouds with Histogram Stretching and Color Table Manipulation

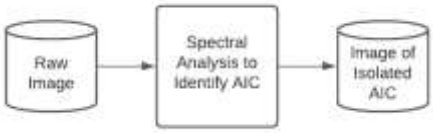

Figure 2. Abridged Method for Hyperspectral Analysis of AIC

Image preprocessing and analysis were completed with the Imagery Analysis Remote Sensing Tool, L3 Harris ENVI Classic version 5.5.3.

Step 1: Eliminate Noisy Bands

An image from AVIRIS Classic inherently contains 224 bands. Using the band animation tool, it is possible to efficiently view each band and determine and take note of which ones are bad (noisy, unreadable). Then, it is necessary to remove these bad bands by editing the image header file which may be accomplished within ENVI. For this image, preprocessing identified 61 bad bands. These were removed from the hypercube, leaving 163 bands used for this analysis.

Step 2: Identify and Overlay Regions of Interest

In *Aviation Sustainability Through Hyperspectral Image Analysis Methodology for Aircraft-Induced Clouds*, 5 regions of interest (ROIs) are established: cumulus clouds, thin altostratus clouds, medium altostratus clouds, roads, and light patches. The primary regions of interest are the cumulus and altostratus clouds in the image, the latter being broken down into thin and medium altostratus where thin and medium refer to optical depth. In addition to the clouds, the ROIs account for areas that may be misinterpreted by algorithms for clouds such as the light-colored roads and patches throughout the image.

ROI Name	Color	Pixels	Polygons	Polylines	Points	Fill	Orien	Space
Cumulus	Blue1	1,909	1/1,909	0/0	0	Solid	45	0.10
Thin Altostratus	Thistle1	103	2/103	0/0	0	Solid	45	0.10
Medium Altostratus	Thistle2	144	1/144	0/0	0	Solid	45	0.10
Road	Black	111	0/0	0/0	111	Solid	45	0.10
Light Patch	Yellow	99	0/0	0/0	99	Solid	45	0.10

Figure 3. Regions of Interest (ROI)

Preparation for exploitation-ready imagery involved creating a library of in-scene regions of interest (ROI), whose spectral signatures are graphed in Figure 4.

In addition to the clouds, the ROIs account for areas that may be misinterpreted by algorithms for clouds, such as the light-colored roads and patches throughout the image.

Figure 4 shows the Endmember Collection Spectra which graphically displays which wavelengths uniquely define spectra by maxima and minima.

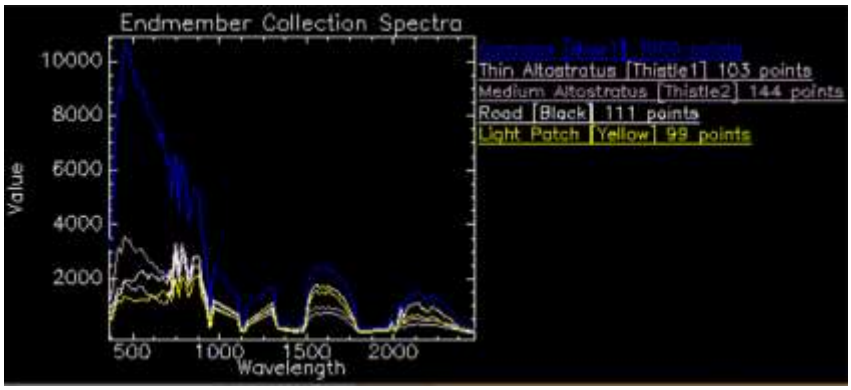

Figure 4. ROI Spectral Signatures

Step 3: Create Spectral Library Based on In-scene Spectra

A spectral library identifies the unique spectral characteristics for each type of cloud. The spectra are used to identify the objects of interest in the image.

An in-scene spectral library defines the spectral properties of substances and may serve to detect and identify and locate the substances throughout a scene. Additionally, the spectral signatures may be plotted across the electromagnetic spectrum for comparison. Spectrally similar substances have similar plot shapes. Figure 4 has layered spectra of the in-scene library. The wavelength range covers 400 to 2,500 nanometers on the horizontal axis and radiance is represented on the vertical axis. Radiance is directly measured by the AVIRIS sensor and uses the units Watt/(steradian/meter^2).

There are no publicly available spectral libraries for clouds which limits research in remote sensing of clouds.

Step 4: Run Algorithms (MF, ACE, PCA) with In-Scene Spectra on Image

The 3 algorithms used in this study are the ENVI Matched Filter (MF), Adaptive Coherence Estimator (ACE), and Principal Components Analysis (PCA).

Matched Filter (MF)

The Matched Filter (MF) algorithm uses the In-scene Spectral Library from Step 3 to identify the object in the image.

MF provides the same kind of output as ACE, however in eigenvector form. It is generally regarded as being more effective in discarding non-target spectra than ACE. Similar to ACE, high values in the histogram represent near-target and target results. Additionally like ACE, MF is statistically-based. However, the increased sensitivity to the target signal has the tendency to yield more false positive results. The units are dimensionless and represented as a real number between 0 and 1, inclusive. The formula for which is expressed in Equation 1 where ρ_a represents the spectrum of interest, m is the background, and ρ_b is the pixel under-test (PUT). The

numerator is similar to Mahalanobis Distance and the denominator is scalar.

$$Matched\ Filter = \frac{(\rho_a^T m^{-1} \rho_b)}{(\rho_a^T m^{-1} \rho_a^T)}$$

Equation 1. Matched Filter Equation [18]

Adaptive Coherence Estimator (ACE)

An alternative to MF can be accomplished with ACE. The ENVI ACE algorithm is a statistics-based tool which provides a pixel decomposition and determination of composition percentage within the pixels. It can be considered a cosine squared-normalized matched filter where eigenvectors should be orthogonal. The exception to this norm is singularity which is difficult to decompose thus creating an issue of collinearity. [19]

Principal Components Analysis (PCA)

ENVI PCA is a second order statistics-based data transformation where second order refers to covariance. Attributes such as spectral minimum, maximum, mean, and standard deviation are normalized for zero mean and unit variance. PCA computes both eigenvalues and eigenvectors. PCA is typically used as a data reconnaissance, quality control, and anomaly detection method. It works best after conservative removal of noisy bands. Attribute transformation into principal component space is based on principal eigenvectors corresponding to non-zero eigenvalues. [20]

Step 5: Isolate Clouds with Histogram Stretching and Color Table Manipulation

Interactively stretching the histogram, giving preference to higher values, gets pixels brighter or darker as a response to the percentage value of the pixel.

Histogram stretching is also known as input cropping. It is a linear transformation which expands part of the original histogram, the extent to which is determined by the user. Thus, the nonzero intensity range occupies the full dynamic grayscale represented by Equation 2 where *S* represents the subset of pixels in an image determined by the user, *r* represents function intensity, and *L* represents the number of intensity levels and may be calculated by Equation 3 where *k* represents an integer between 0 and *L*-1 as calculated by dividing the number of bits by pixel.

$$S = \frac{r - r_{min}}{r_{max} - r_{min}} \times (L - 1)$$

Equation 2. Histogram Stretching

$$L = 2^k$$

Equation 3. Intensity Level

[21]

Lastly, the color tables may be stretched and set to different color schemes. In accordance with color theory, it is recommended to represent clouds as white as it is the most inherently understandable as clouds are typically white in nature. For most ease in data visualization, the isolated clouds shown in the results are portrayed on a black background.

4 RESULTS – CASE STUDY

Images were processed using the Matched Filter (MF), Adaptive Coherence Estimator (ACE), and Principal Components Analysis (PCA) algorithms. A goal of this paper is to determine the usability of these algorithms based on naturally formed cumulus and altostratus clouds for applications of AIC. Figures show results in 2 displays. Display 1 is on the left and is a color composite red-green-blue (RGB) image one bands 183, 193, 207 representing wavelengths 2.10µm, 2.20µm, and 2.35µm, respectively. The ROIs are overlaid in Display 1 and their colors correspond to those shown in Figure 3. Display 2 is on the right and shows the results of the respective algorithms. The topmost images show the cumulus cloud, the middle images show the thin altostratus clouds, and the bottommost images show the medium altostratus clouds.

The histogram for the MF cumulus cloud is stretched to the range 0.198-1.605, the thin altostratus is stretched to 0.464-2.162, and the medium altostratus is stretched to 0.233-1.602. The cumulus cloud was completely isolated and kept textural nuance of the cloud resulting from cumuliform development. The "fluffy" nature of cumulus clouds was slightly lost in the top-down view of the AVIRIS sensor and due to high illumination. None of the surrounding roads or patchy areas were activated, indicating good ROI selection. This is an example of potential benefit of the development of an additional ROI representing shadowed cumulus areas. The thin altostratus results picked up minor traces of the road. Adjusting the histogram to be more tolerant would allow for the appearance of more optically thin altostratus clouds, however it would exacerbate the presence of the road. The medium altostratus results showed the textural nuance (wispy nature of altostratus clouds) well.

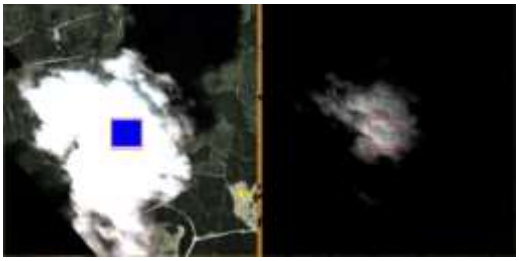

Cumulus Cloud Region of Interest with Results of Matched Filter

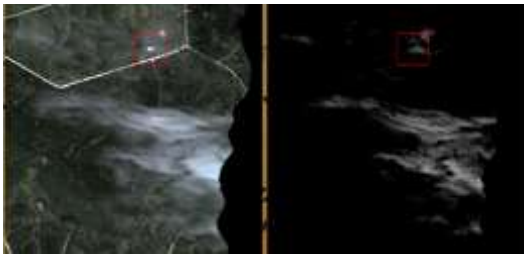

Thin Altostratus Cloud Region of Interest with Results of Matched Filter

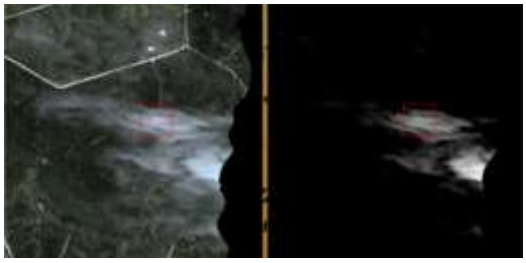

Medium Altostratus Cloud Region of Interest with Results of Matched Filter

Figure 5. MF Results

The histogram for the ACE cumulus cloud is stretched to the range 0.007-0.379, the thin altostratus is stretched to 0.022-0.350, and the medium altostratus is stretched to 0.014-0.504. The cumulus cloud was completely isolated; however, ACE is more selective than MF, resulting in lost "volume" of the cumulus cloud. None of the surrounding roads or patchy areas were activated, indicating good ROI selection. This is an example of potential benefit of the development of an additional ROI representing shadowed cumulus areas. The thin altostratus picked up on more thin altostratus clouds and still no roads or the cumulus cloud. The medium altostratus results were similar to that from MF.

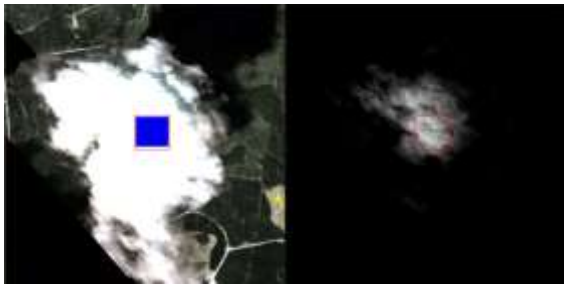

Cumulus Cloud Region of Interest with Results of Adaptive Coherence Estimator

Thin Altostratus Cloud Region of Interest with Results of Adaptive Coherence Estimator

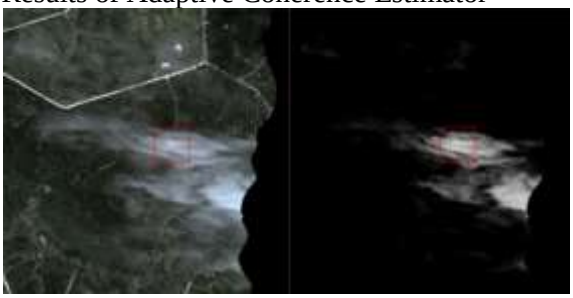

Medium Altostratus Cloud Region of Interest with Results of Adaptive Coherence Estimator

Figure 6. ACE Results

4.3 PCA

The histogram for the PCA cumulus cloud is stretched to the range –25,600.615 to 2,732.093 on band 1, the thin altostratus is stretched to -195.619 to 67.109 on band 10, and the medium altostratus is stretched to –215.828 to 67.109 also on band 10. The cumulus cloud was completely isolated. However, the thin altostratus clouds picked up all the medium altostratus clouds as well as some Earth surface components. The medium altostratus clouds picked up the cloud cores well and left out the thin altostratus.

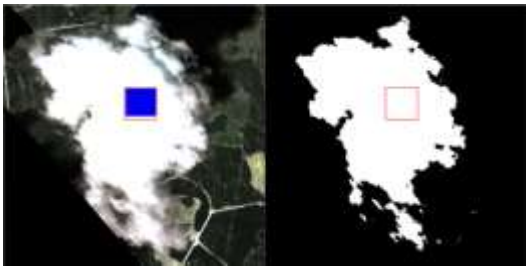

Cumulus Cloud Region of Interest with Results of Principal Components Analysis

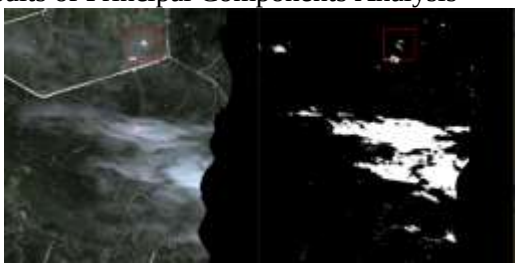

Thin Altostratus Region of Interest with Results of Principal Components Analysis

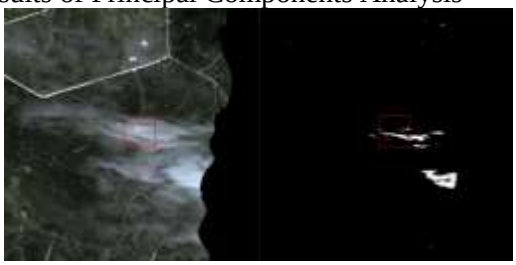

Medium Altostratus Cloud Region of Interest with Results of Principal Components Analysis

Figure 7. PCA Results

5 CONCLUSIONS

This paper describes a method for hyperspectral analysis of remotely sensed aerial images to identify AIC based on the analysis of altostratus and cumulus clouds. The method eliminates noisy bands, identifies and overlays primary regions of interest, creates a spectral library based on in-scene spectra, runs algorithms (MF, ACE, PCA from ENVI Classic 5.5.3) with in-scene spectra on image, and isolates clouds with histogram stretching and color table manipulation. The process is demonstrated with an aerial image from AVIRIS Classic flight f100906t01, Donaldson Plantation Flight Line 1 over Gainesville, Florida on September 6, 2010 at 18:29 UTC (14:29 EDT).

The Matched Filter was the most effective in isolating cloud types, based on in-scene spectra created by the user. The independent cumulus cloud was the most easily identified and processed image results showed the sharpest edges. This area could benefit from an additional ROI depicting the shaded regions of the cumulus cloud, given that

hyperspectral remote sensing is sensitive to illumination and yields higher quality results in uniformly illuminated areas.

Matched Filter, in addition to the Adaptive Coherence Estimator and Principal Components Analysis, should be applied to remotely-sensed hyperspectral imagery of AIC, and additionally coupled with an overlay of flight tracks and atmospheric data to increase the confidence index of AIC identification.

Future Work

Future work in utilizing hyperspectral imagery for AIC detection and identification lies primarily in increasing the confidence index by overlaying isolated AIC with flight tracks fused with atmospheric data on ice supersaturated regions and labels from machine learning.

REFERENCES

[1] Lee, D. S., D.W. Fahey, A. Skowron, M.R. Allen, U. Burkhardt, Q. Chen, L.J. Wilcox, 2021, The contribution of global aviation to anthropogenic climate forcing for 2000 to 2018. Atmospheric Environment, 244, 117834.

[2] Kärcher, B, 2018, Formation and radiative forcing of contrail cirrus, Nature Communications, 9(1), 1824 https://doi.org/10.1038/s41467-018-04068-0.

[3] Avila, Denis, Lance Sherry, Terry Thompson, 2019, Reducing global warming by airline contrail avoidance: A case study of annual benefits for the contiguous United States, Transportation Research Interdisciplinary Perspectives, 2, 100033 https://doi.org/10.1016/j.trip.2019.100033.

[4] Teoh, R., Ulrich Schumann, A. Majumdar, M.E.J Stettler, 2020, Mitigating the Climate Forcing of Aircraft Contrails by Small-Scale Diversions and Technology Adoption, Environmental Science & Technology, 54(5), 2941–2950 https://doi.org/10.1021/acs.est.9b05608.

[5] Rosenow, Judith, H. Fricke, T. Luchkova, M. Schultz, 2018, Minimizing contrail formation by rerouting around dynamic ice-supersaturated regions, Aeronautics and Aerospace Open Access Journal, 2 https://doi.org/10.15406/aaoaj.2018.02.00039.

[6] Kaiser, M., Judith Rosenow, H. Fricke, M. Schultz, 2012. Tradeoff between optimum altitude and contrail layer to ensure maximum ecological en-route performance using the enhanced trajectory prediction model (ETPM) (p. 134).

[7] Sherry, Lance, Terry Thompson, 2020, Primer on Aircraft Induced Clouds and Their Global Warming Mitigation Options, Transportation Research Record, 2674(11), 827–841, https://doi.org/10.1177/0361198120951188.

[8] AVIRIS - airborne visible / infrared Imaging Spectrometer, NASA, https://aviris.jpl.nasa.gov/.

[9] Burkhardt, U., & B. Kärcher, 2011, Global radiative forcing from contrail cirrus, Nature Climate Change, 1(1), 54–58, https://doi.org/10.1038/nclimate1068.

[10] Kaiser, M., Judith Rosenow, H. Fricke, M. Schultz, 2012, Tradeoff between optimum altitude and contrail layer to ensure maximum ecological en-route performance using the enhanced trajectory prediction model (ETPM), p. 134.

[11] Kärcher, B, 2018, Formation and radiative forcing of contrail cirrus, Nature Communications, 9(1), 1824. https://doi.org/10.1038/s41467-018-04068-0.

[12] Kärcher, B., J. Kleine, D. Sauer, C. Voigt, 2018, Contrail Formation: Analysis of Sublimation Mechanisms, Geophysical Research Letters, 45(24), 13,547-13,552, https://doi.org/10.1029/2018GL079391.

[13] Newinger, C., U. Burkhardt, 2012, Sensitivity of contrail cirrus radiative forcing to air traffic scheduling, Journal of Geophysical Research, Atmospheres, 117(1) http://dx.doi.org/10.1029/2011JD016736.

[14] Schröder, F., B. Kärcher, C. Duroure, J. Ström, A. Petzold, J.F. Gayet, B. Strauss, P. Wendling, S. Borrmann, 2000, On the Transition of Contrails into Cirrus Clouds. Journal of the Atmospheric Sciences, 57(4), 464–480, https://doi.org/10.1175/1520-0469(2000)057<0464:OTTOCI>2.0.CO;2.

[15] Schumann, Ulrich, 1996, On Conditions for Contrail Formation from Aircraft Exhausts, Meteorologische Zeitschrift, 5, 4–23.

[16] Schumann, Ulrich, A.J. Heymsfield, 2017, On the Life Cycle of Individual Contrails and Contrail Cirrus, Meteorological Monographs, 58(1), 3.1-3.24, https://doi.org/10.1175/AMSMONOGRAPHS-D-16-0005.1

[17] Avila, Denis, Lance Sherry, 2016, Method for analysis of Ice Super Saturated Regions (ISSR) in the U.S. airspace, 2016 Integrated Communications Navigation and Surveillance (ICNS), pp. 10B2-1-10B2-9, https://doi.org/10.1109/ICNSURV.2016.7486319.

[18] Matched Filtering, https://www.l3harrisgeospatial.com/docs/matchedfiltering.html.

[19] Adaptive Coherence Estimator, https://www.l3harrisgeospatial.com/docs/adaptivecoherenceestimator.html.

[20] Principal Components Analysis, https://www.l3harrisgeospatial.com/docs/principalcomponentanalysis.html.

[21] Gonzalez, Rafael, Richard Woods, 2008, Intensity Transformations and Spatial Filtering, Digital image processing, 4th ed., Pearson Education Limited.

ACKNOWLDGEMENTS

The authors acknowledge the help of Dr. Ron Resmini (L3 Harris) in providing access to the ENVI software and Dr. Donglian Sun (George Mason University) and Dr. Edward Oughton (George Mason University) for their support.

EMAIL ADDRESSES

arose20@gmu.edu

lsherry@gmu.edu

2022 Integrated Communications Navigation and Surveillance (ICNS) Conference

April 5-7, 2022